

An optically pumped GaN/AlGaIn quantum well intersubband terahertz laser

This article has been downloaded from IOPscience. Please scroll down to see the full text article.

2013 Chinese Phys. B 22 026803

(<http://iopscience.iop.org/1674-1056/22/2/026803>)

View [the table of contents for this issue](#), or go to the [journal homepage](#) for more

Download details:

IP Address: 219.228.112.158

The article was downloaded on 28/02/2013 at 15:54

Please note that [terms and conditions apply](#).

An optically pumped GaN/AlGaIn quantum well intersubband terahertz laser*

Fu Ai-Bing(傅爱兵), Hao Ming-Rui(郝明瑞), Yang Yao(杨耀), Shen Wen-Zhong(沈文忠)[†], and Liu Hui-Chun(刘惠春)[‡]

Key Laboratory of Artificial Structures and Quantum Control (Minister of Education), Department of Physics, Shanghai Jiao Tong University, Shanghai 200240, China

(Received 2 July 2012; revised manuscript received 22 August 2012)

We propose an optically pumped nonpolar GaN/AlGaIn quantum well (QW) active region design for terahertz (THz) lasing in the wavelength range of 30 μm \sim 40 μm and operating at room temperature. The fast longitudinal optical (LO) phonon scattering in GaN/AlGaIn QWs is used to depopulate the lower laser state, and more importantly, the large LO phonon energy is utilized to reduce the thermal population of the lasing states at high temperatures. The influences of temperature and pump intensity on gain and electron densities are investigated. Based on our simulations, we predict that with a sufficiently high pump intensity, a room temperature operated THz laser using a nonpolar GaN/AlGaIn structure is realizable.

Keywords: quantum well structure, intersubband terahertz laser, GaN

PACS: 68.65.Fg, 42.55.Px, 61.72.uj

DOI: 10.1088/1674-1056/22/2/026803

1. Introduction

The terahertz frequency (THz) range (wavelengths from 30 μm to 1000 μm) remains one of the least developed spectral regions,^[1] although a surge of activity in the past decade has advanced its potential for applications including astrophysics and atmospheric science, biological and medical science, security screening and illicit material detection, non-destructive evaluation, communications technology, and spectroscopy.^[2–5] In 1971 Kazarinov and Suris proposed a laser based on intersubband transitions in quantum wells (QWs).^[6] The first quantum cascade laser (QCL) was demonstrated at a wavelength of 4.3 μm (frequency of 70 THz) in 1994.^[7] Seven years later in 2002 the first THz QCL was reported with a lasing frequency of 4.4 THz (wavelength of 68 μm).^[8] Presently research on terahertz lasers is progressing at a rapid pace.

Although the first THz QCL operated up to a maximum temperature of $T_{\text{max}} = 50$ K and improvements in active regions and waveguides brought about substantial progress in GaAs/AlGaAs-based QCL working temperature ($T_{\text{max}} = 199.5$ K),^[9–11] room-temperature operation of THz lasers will require an additional revolution either through the invention of an alternative active region design, or through the use of a new system. Thermal backfilling is one of the major processes causing a degradation of population inversion in THz QCLs at high temperatures.^[1] The thermal backfilling process works as follows: backfilling of the lower radiative state with electrons from the heavily populated ground state occurs by thermal ex-

citation (roughly according to Boltzmann distribution). In a GaAs-based material system, in order to take advantage of the rapid resonant longitudinal optical (LO) phonon scattering depopulation, the energy separation between the lower laser state and the ground state is just above the LO phonon energy^[12] (~ 36 meV), which is comparable to room temperature $k_{\text{B}}T$ (~ 26 meV). In addition, QCLs based on semiconductors such as GaAs/AlGaAs are not capable of emitting in the energy range around the LO phonon energies ($E_{\text{LO}} \sim 36$ meV in GaAs), leaving a gap in the spectral range between 30 μm and 40 μm .^[13]

Obviously, a material system with large LO phonon energy will be advantageous. In contrast to a QCL, which is electrically pumped, optically pumped intersubband lasing has received limited attention so far. Optical pumping offers the advantage of highly selective excitation of carriers into the desired subband and thus provides a tool for the study of lasing mechanisms, carrier relaxation, and other processes.^[14] Compared with a GaAs material system, a GaN material system has a larger LO phonon energy (~ 90 meV). Its alloys with aluminum nitride and related quantum wells have attracted significant attention in recent years, resulting in many successful advances^[15–17] based on this material system. Previous attempts to grow nonpolar GaN by vapor phase and molecular beam epitaxy yielded rough and faceted surfaces that were unsuitable for use in practical devices. Beginning with Waltereit *et al.*'s work,^[18] significant progress has been made in improving nonpolar GaN structure quality and morphology.^[19,20] We present a design and simulation of an optically pumped nonpo-

*Project supported in part by the National Major Basic Research Program of China (Grant No. 2011CB925603) and the Shanghai Municipal Major Basic Research Project (Grant No. 09DJ1400102).

[†]Corresponding author. E-mail: wzshen@sjtu.edu.cn

[‡]Corresponding author. E-mail: h.c.liu@sjtu.edu.cn

lar GaN/AlGaIn QW THz laser. This laser could work at room temperature with a sufficiently high pump intensity. Moreover it can emit at energy of 36.3 meV (about 8.7 THz), which is beyond the capability of GaAs lasers.

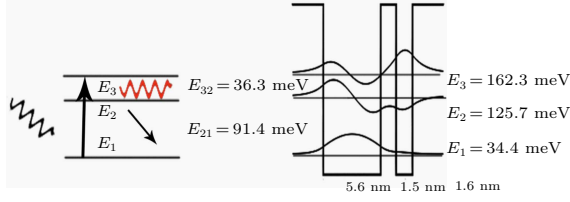


Fig. 1. (color online) Right: calculated double quantum well potential and wave functions; left: illustration of the optically pumped nonpolar laser. E_3-E_1 is tuned for CO₂ laser pumping, and terahertz emission is generated from E_3 to E_2 transitions.

Figure 1 shows the active region of the proposed nonpolar AlGaIn/GaN laser structure which consists of three Al_{0.15}Ga_{0.85}N barriers and two GaN wells. In this three-level laser system, levels E_3 and E_2 are the upper and the lower laser states, respectively. The laser operates as follows: electrons are pumped into the upper laser state E_3 ; undergo a lasing transition to the lower laser state E_2 ; and then a depopulation of E_2 occurs by scattering with LO phonon to ground state E_1 . A detailed investigation of the performance of this structure is also presented. In the following sections, we first introduce the theoretical model for this system and then calculate the transition time for each process, after that we use the rate equation consideration to obtain the electron densities for all subbands, and finally we present the results with discussion.

2. Theoretical model

2.1. Electron transition rate by interaction with phonon

The transition rate for scattering an electron from initial subband i with in-plane wave vector \mathbf{k} into any state in subband j via the interaction with phonon is calculated by Fermi's golden rule

$$W_{ij}(k) = \frac{2\pi}{\hbar} \int |\langle k', j | H_{ep} | k, i \rangle|^2 \delta(E_{k',j} - E_{k,i} \mp \hbar\omega_Q) dN_{k'}, \quad (1)$$

where H_{ep} is the electron-phonon interaction Hamiltonian, $E_{k,i}$ is the energy for state $|k, i\rangle$ in subband i , which can be

$$W_{ij}(k) = \frac{2\pi}{\hbar} \int \left\{ |\langle k', j | H_{ep} | k, i \rangle|^2 \left[\int_{-1}^1 \delta\left(\frac{\hbar^2 q^2}{2m^*} + \frac{\hbar^2 kq}{2m^*} \cos\theta + E_i - E_j \mp \hbar\omega_Q\right) \frac{d\cos\theta}{\sqrt{1-\cos^2\theta}} \right] 2q dq \right\} dq_z. \quad (7)$$

(i) Acoustical phonon scattering: the energies of acoustical phonons are in general small and may be neglected,

$$\hbar\omega_Q \approx 0. \quad (8)$$

The scattering rate by acoustical phonons from subband i into

written as

$$E_{k,i} = E_i + \frac{\hbar^2 k^2}{2m^*}, \quad (2)$$

m^* is the electron effective mass in GaN, $\hbar\omega_Q$ is the phonon energy, and the integration is over all final states to which the scattering process is allowed by energy conservation and in-plane momentum conservation.

The phonon wave vectors have been decomposed into their in-plane and normal components, as $\mathbf{Q} = \mathbf{q} + q_z \mathbf{e}_z$. The transition rate integral can be evaluated by transforming the integral over final states to one over \mathbf{Q} , $dN_{k'} = [\Omega/(2\pi)^3] q dq d\theta dq_z$. Ω is the volume of the sample. The matrix element can be expressed as follows:^[21]

$$|\langle k', j | H_{ep} | k, i \rangle|^2 = \begin{cases} \frac{\Xi^2 k_B T}{2c_l \Omega} \delta_{q,\pm(k'-k)} |G_{ij}(q_z)|^2, & \text{acoustical,} \\ \frac{e^2 \hbar \omega_0}{2\varepsilon_p \Omega} \frac{Q^2}{(Q^2 + q_0^2)^2} \delta_{q,\pm(k'-k)} & \\ |G_{ij}(q_z)|^2 [n(\omega_Q) + 1/2 \mp 1/2] & \text{longitudinal optical,} \end{cases} \quad (3)$$

where the upper sign is for absorption and the lower for emission of the phonon; Ξ is the deformation potential; k_B is the Boltzmann constant; c_l is the elastic constant associated with acoustical vibration; e is the free-electron charge; and q_0 is the reciprocal length. $G_{ij}(q_z)$ contains the wave functions interference effects and can be expressed as $G_{ij}(q_z) = \langle j | e^{iq_z z} | i \rangle$. The permittivity constant ε_p is

$$\frac{1}{\varepsilon_p} = \frac{1}{\varepsilon_\infty} - \frac{1}{\varepsilon_s}, \quad (4)$$

where ε_∞ and ε_0 are high-frequency and static permittivity, respectively, and $(n\omega_Q)$ is the equilibrium number of optical phonons

$$n(\omega_Q) = \frac{1}{\exp(\hbar\omega_Q/k_B T) - 1}. \quad (5)$$

The Kronecker symbol in the matrix element represents the in-plane momentum conservation

$$k'^2 = k^2 + q^2 \pm 2kq \cos\theta, \quad (6)$$

where θ is the angle between k and q .

Finally, the transition rate is calculated by the following three-dimensional integral:^[21]

subband j is

$$W_{ij}^a(k) = \frac{\Xi^2 k_B T m^*}{2\pi c_l \hbar^3} \int |G_{ij}(q_z)|^2 dq_z. \quad (9)$$

(ii) LO-phonon scattering: the LO phonon energy can be approximated as a constant $\hbar\omega_Q$. The scattering rate by LO

phonons from subband i into subband j is

$$W_{ij}^0(k) = \frac{e^2 w_0 [n(w_0) + 1/2 \mp 1/2]}{8\pi\epsilon_p} \times \int \frac{|G_{ij}(q_z)|^2}{\left[\frac{\hbar^4 k^2 q_z^2}{m^{*2}} + \left(\frac{\hbar^2 q_z^2}{2m^*} + E_i - E_j \pm \hbar w_Q \right)^2 \right]^{1/2}} dq_z. \quad (10)$$

It is well known that electron–electron scattering becomes relevant only at high carrier concentration and at small spacings (up to 10 meV) between energy levels; hence it should not be too important in this system considered here.^[22–24]

2.2. Interaction of electrons with electromagnetic field

For the z -polarized radiation, the pumping rate is given by^[25]

$$M = \frac{e^2 \pi}{n\epsilon_0 \hbar c} z_{13}^2 \frac{\Gamma}{2\pi} \frac{1}{(\hbar\omega - \hbar\omega_0)^2 + (\Gamma/2)^2} P, \quad (11)$$

where n is the refractive index and Γ is the transition line width taken to be equal to 15% of the transition energy—typical in the THz intersubband lasers.^[1,26–29] $\hbar\omega_0$ and $\hbar\omega$ are the transition and photon energies, respectively, z_{13} is the dipole matrix element

$$z_{13} = \int \varphi_3^* z \varphi_1 dz,$$

$P = \Phi \times \hbar\omega$ is the pump intensity of the pump laser, and Φ is the pump flux.

2.3. Rate equations

The rate equations for a three-level system is

$$\begin{cases} \frac{\partial n_1}{\partial t} = -M_{13}(n_1 - n_3) + \frac{n_3 - n_{3T}}{\tau_{31}} + \frac{n_2 - n_{2T}}{\tau_{21}}, \\ \frac{\partial n_2}{\partial t} = \frac{n_3 - n_{3T}}{\tau_{32}} - \frac{n_2 - n_{2T}}{\tau_{21}}, \\ \frac{\partial n_3}{\partial t} = M_{13}(n_1 - n_3) - \frac{n_3 - n_{3T}}{\tau_{32}} - \frac{n_3 - n_{3T}}{\tau_{31}}, \\ n_1 + n_2 + n_3 = n_{1T} + n_{2T} + n_{3T} = n_s, \end{cases} \quad (12)$$

where n_s is the total electron density and ($n_s = N_D L$) N_D is the doping concentration, L is the effective length of the structure. The thermal population effect in the three-level system is taken into account by allowing n_i to approach n_{iT} , which is the area electron density in subband i assuming thermal equilibrium distribution when the pump light is turned off. They are related by the approximation of Boltzmann distribution.^[17] Equation (12) can be solved in the steady state ($d/dt = 0$), and we then obtain electron density in the laser system.

For a simple analysis, the population n_2 of the second subband is given by

$$\frac{\partial n_2}{\partial t} = \frac{n_3 - n_{3T}}{\tau_{32}} - \frac{n_2 - n_{2T}}{\tau_{21}} \quad (13)$$

in steady state $dn_2/dt = 0$, and noting that $n_{3T} < n_{2T}$, dictated by the Boltzmann distribution. Then the standard necessary

condition for population inversion reads:

$$\frac{1}{\tau_{32}} < \frac{1}{\tau_{21}}. \quad (14)$$

After getting the electron densities in the three laser states of the system, the optical gain is

$$g = \frac{2e^2 \omega}{n\epsilon_0 \Gamma c} z_{23}^2 \frac{n_3 - n_2}{L}. \quad (15)$$

3. Results and discussion

A range of double quantum wells with $\text{Al}_x\text{Ga}_{1-x}\text{N}$ barriers of the same x and GaN wells were investigated. The length of the outer barriers was set to a fixed value of 10 nm, while the inner barrier width L_b , left and right well widths L_1 and L_2 , and the Al content in the barrier x were varied. Calculations were performed for various n_s values and results for $n_s = 10^{12} \text{ cm}^{-2}$ are presented. Figure 1 shows the active region of the proposed AlGaIn/GaN laser structure. Electrons are pumped into the upper laser state E_3 ; undergoing a lasing transition to lower laser state E_2 ; and then depopulating by scattering with LO phonon to ground state E_1 . The photon energy generated from the lasing transition is 36.3 meV corresponding to 8.7-THz radiation (34.2 μm) which ordinary QCLs based on GaAs/AlGaAs cannot cover. The energy separation between levels E_2 and E_1 is designed to be 91.4 meV, just above the GaN LO phonon energy.^[30] (~ 90 meV), such that depopulation of lower laser state E_2 is rapid through the near-resonant LO-phonon emission process yielding a very short lifetime τ_2 for the lower laser state E_2 . The larger spatial separation between levels E_3 and E_1 , on the other hand, leads to a longer lifetime τ_3 for the upper laser state E_3 .

In order to solve the rate equation (12), the scattering time is needed. The scattering times (reciprocal of scattering rate W_{ij}) of subbands are determined by these scattering mechanisms: LO phonon, acoustic phonon, electron–electron, interface roughness, and impurity scattering processes. Although the interface roughness and impurity scattering are expected to play an important role in nonpolar GaN-based lasers, for simplicity we have not included these effects as they depend on actual structure qualities.^[17] The scattering time related to absorbing an acoustic phonon are on the order of 10^5 ps which is too long, thus we can neglect it. We can explain this by simple physical argument. The acoustic phonon energy is near zero and the electrons are mostly on the bottom of a subband. If it absorbs an acoustic phonon (near zero energy), the electrons cannot go up to another subband. We therefore do not need to consider the rate due to absorbing an acoustic phonon. Since electrons from the bottom of the third subband cannot emit an LO phonon to subband E_2 because of the energy conservation,

the interaction with acoustic phonon is dominant in the E_3 to E_2 transition process. Moreover, because of the energy conservation and the high pump rate by CO₂ laser, we can ignore the scattering rate related to absorbing a phonon from the subband E_1 to subband E_3 .

The scattering rate results for the structure at the temperature 77 K are summarized in Table 1, which lists the total scattering rate W_{ij} from the subband i to subband j . The scattering rate from E_2 to E_1 is 37.5 ps⁻¹, which is significantly larger than that from E_3 to E_2 (0.11 ps⁻¹) and essential to achieve population inversion according to Eq. (14). The energy difference between subband E_3 and E_1 (127.7 meV) is larger than that between E_2 and E_1 (91.4 meV) which is close to the LO phonon energy 90 meV. As a result, the scattering rate from E_3 to E_1 (8.17 ps⁻¹) is smaller than the rate from E_2 to E_1 . According to formula (5), there are very few LO phonons at temperature 77 K, so the scattering rate for an electron absorbing an LO phonon from the subband E_2 to E_3 is very small, shown in table E_1 (about 3.977×10^{-5} ps⁻¹). Table 2 shows the scattering rate via interaction with phonons for $T = 300$ K. It is interesting to note that the scattering rates from E_1 to E_2 and from E_2 to E_3 rise dramatically with temperature. This is related to the increase in LO phonon absorbing rate caused by the increase in the phonon population at high temperature.

Table 1. Calculated scattering rate with pump intensity of 8 MW/cm² at temperature of liquid nitrogen (77 K).

W_{ij}/ps^{-1}	$j=1$	$j=2$	$j=3$
$i=1$	0	5.09×10^{-5}	0
$i=2$	37.50	0	3.98×10^{-5}
$i=3$	8.17	0.12	0

Table 2. Calculated scattering rate with pump intensity of 8 MW/cm² at room temperature (300 K).

W_{ij}/ps^{-1}	$j=1$	$j=2$	$j=3$
$i=1$	0	1.24	0
$i=2$	38.94	0	0.97
$i=3$	8.55	0.45	0

All calculated scattering times decrease with temperature as the phonon numbers increase for higher temperature. The effective lifetimes for the upper and lower laser states are given by $1/\tau_3 = 1/\tau_{31} + 1/\tau_{32}$ and $1/\tau_2 = 1/\tau_{21} + 1/\tau_{23}$. It can be seen from Fig. 2 that τ_2 and τ_{21} are nearly the same in a low temperature range but deviate somewhat after 170 K. This is caused by the fact that the fast depopulation process from E_2 to E_1 via near-resonant LO-phonon emission determines the process between E_2 and E_1 , but when the temperature becomes high, the scattering time from E_2 to E_3 absorbing an LO-phonon decreases, having an effect on the τ_2 . The much shorter lifetime of the lower laser state E_2 due to the fast near-

resonant LO-phonon emission process ensures the population inversion.

After getting the scattering time, we can now solve the rate equation (12) and establish the population distribution of this three-level system. Then an investigation of the temperature and pump intensity influence on this system in order to estimate laser performance is available. Figure 3 shows the temperature dependence of the electron densities and the gain. We see that the gain is still larger than required to compensate the losses found within laser cavities, even at 300 K. The result indicates that a room temperature operated QW nonpolar GaN laser is possible. It is seen in this picture the electron densities in subband E_3 and subband E_1 do not change with temperature appreciably, showing a slight decrease. The electron density in subband E_2 is greatly influenced by temperature. In a low temperature range, it increases quickly because of the thermal equilibrium effect and the decrease of transition time τ_{32} . For high temperatures it increases by the combined effect of the decrease of transition times τ_{32} and τ_{12} .

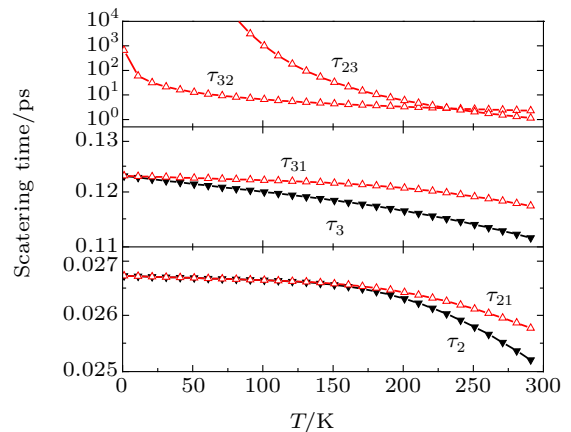


Fig. 2. (color online) Temperature dependence of the transition time for the structure from Fig. 1. Lifetimes of subband E_2 and subband E_1 are also shown.

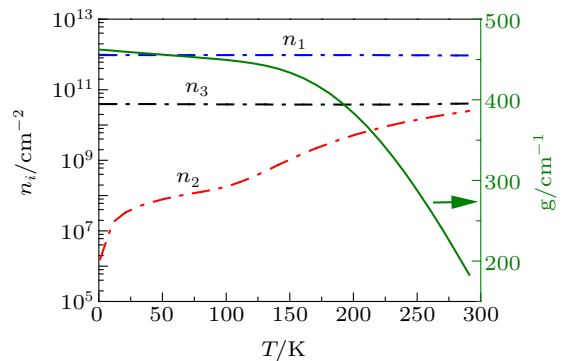


Fig. 3. (color online) Temperature dependence of electron densities and gain at pump intensity $P = 8$ MW/cm² and $n_s = 10^{12}$ cm⁻².

We now compare the laser characteristics at two typical temperatures. Figure 3 shows the situation at 77 K (the liquid

nitrogen temperature). n_3 is linearly dependent on the pump intensity P and n_1 decreases slightly as the pump intensity increases until $P = 100 \text{ MW/cm}^2$ when n_3 approaches n_1 and the population inversion saturates. If we compare Fig. 3 and Fig. 4, we find that n_3 is mostly determined by pump intensity. When the pump intensity is low (10 W/cm^2 – 10 kW/cm^2), n_2 is mostly determined by the thermal equilibrium effect and it remains nearly unchanged. When the pump intensity is higher than 10 kW/cm^2 , results from our simulation show that n_2 increases as the pump intensity continues to increase. When the pump intensity is low (less than 200 W/cm^2) n_2 is greater than n_3 and there is no population inversion. At slightly higher pump intensity, population inversion occurs. In the range from $P = 1 \text{ kW/cm}^2$ to $P = 100 \text{ MW/cm}^2$, the gain depends linearly on the pump intensity. After 100 MW/cm^2 , the gain saturates.

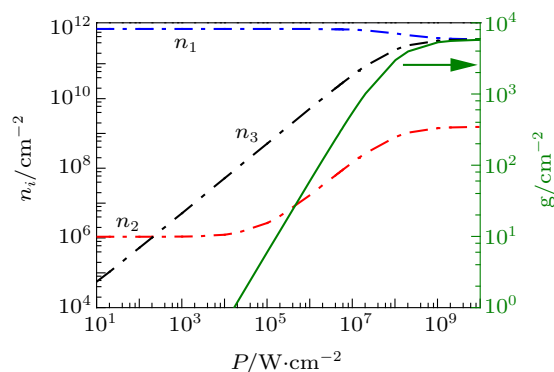


Fig. 4. (color online) Pump intensity dependence of electron densities and gain at temperature $T = 77 \text{ K}$.

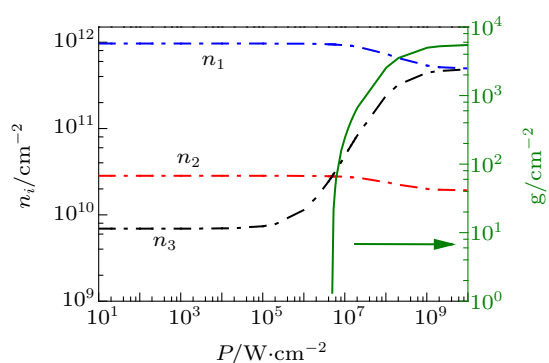


Fig. 5. (color online) Pump intensity dependence of electron densities and gain at temperature $T = 300 \text{ K}$.

Figure 5 shows the pump intensity dependence of electron densities and gain at 300 K . n_1 changes much as it does in Fig. 4. The change of n_2 and n_3 is much different from that at 77 K . n_2 does not increase; instead it decreases when the pump intensity is high, above 4 MW/cm^2 . And n_3 does not increase until the pump intensity reaches 20 kW/cm^2 . The largest difference between Fig. 4 and Fig. 5 is the population inversion point. At 300 K , beyond 5 MW/cm^2 population inversion occurs and the gain begins to be larger than zero as

shown in Fig. 5, which also means the laser needs a stronger pump intensity for high temperature.

4. Conclusions

The purpose of this investigation is to provide a design of a $30 \mu\text{m} \sim 40 \mu\text{m}$ laser source operating at room temperature. An optically pumped nonpolar GaN/AlGaIn QW active region structure for THz lasing at $\lambda = 34 \mu\text{m}$ (in the GaAs reststrahlen region) is presented. The large LO-phonon energies in GaN material system make it possible to achieve room temperature operation. The THz intersubband laser under consideration is a three-level system and the active region of the laser structure consists of multiple periods of two nonpolar GaN QWs coupled by an $\text{Al}_{0.15}\text{Ga}_{0.85}\text{N}$ barrier. The laser rate equations were solved with both LO and acoustical phonon scattering and the thermal equilibrium effect taken into consideration. The influence of temperature on values of gain and electron densities with fixed pump intensity of 8 MW/cm^2 was investigated and we predict that at room temperature, the structure still has a gain value of about 150 cm^{-1} . We analyzed the performance of designed structure with varying pump intensities at two typical temperatures. Based on our simulations, we predict that at a pump intensity of 8 MW/cm^2 , a room temperature operated THz laser using the nonpolar GaN/AlGaIn structure is realizable.

References

- [1] Williams B S 2007 *Nature Photonics* **1** 517
- [2] Kim S M, Hatami F, Harris J S, Kurian A W, Ford J, King D, Scalfari G, Giovannini M, Hoyler N, Faist J and Harris G 2006 *Appl. Phys. Lett.* **88** 153903
- [3] Barbieri S, Alton J, Baker C, Lo T, Beere H and Ritchie D 2005 *Opt. Express* **13** 6497
- [4] Nguyen K L, Johns M L, Gladden L, Worrall C H, Alexander P, Beere H E, Pepper M, Ritchie D A, Alton J, Barbieri S and Linfield E H 2006 *Opt. Express* **14** 2123
- [5] Lee A W M, Williams B S, Kumar S, Hu Q and Reno J L 2006 *IEEE Photon. Technol. Lett.* **18** 1415
- [6] Kazarinov R and Suris R 1971 *Sov. Phys. Semicond.* **5** 707
- [7] Faist J, Capasso F, Sivco D L, Sirtori C, Hutchinson A L and Cho A Y 1994 *Science* **264** 553
- [8] Köler R, Tredicucci A, Beltram F, Beere H E, Linfield E H, Davies A G, Ritchie D A, Iotti R C and Rossi F 2002 *Nature* **417** 156
- [9] Luo H, Laframboise S R, Wasilewski Z R, Aers G C, Liu H C and Cao J C 2007 *Appl. Phys. Lett.* **90** 041112
- [10] Kumar S, Hu Q and Reno J L 2009 *Appl. Phys. Lett.* **94** 131105
- [11] Fatholouloumi S, Dupont E, Chan C, Wasilewski Z, Laframboise S, Ban D, Mátyás A, Jirauschek C, Hu Q and Liu H 2012 *Opt. Express* **20** 3866
- [12] Williams B S, Callebaut H, Kumar S, Hu Q and Reno J L 2003 *Appl. Phys. Lett.* **82**
- [13] Jovanovi V, Indjin D, Ikoni Z and Harrison P 2004 *Appl. Phys. Lett.* **84** 2995
- [14] Liu H C, Song C Y, Wasilewski Z R, Spring-Thorpe A J, Cao J C, Dharma-Wardana C, Aers G C, Lockwood D J and Gupta J A 2003 *Phys. Rev. Lett.* **90** 77402
- [15] Xie G, Xu Edward, Niloufar Hashemi, Zhang B, Fred Y F and Wai T N 2012 *Chin. Phys. B* **21** 086105
- [16] Lü Y J, Lin Z J, Yu Y X, Meng L G, Cao Z F, Luan C B and Wang Z G 2012 *Chin. Phys. B* **21** 097104

- [17] Sun G, Soref R A and Khurgin J B 2005 *Superlattices and Microstructures* **37** 107
- [18] Waltereit P, Brandt O, Trampert A, Grahn H, Menniger J, Ramsteiner M, Reiche M and Ploog K 2000 *Nature* **406** 865
- [19] Craven M D, Lim S H, Wu F, Speck J S and DenBaars S P 2002 *Appl. Phys. Lett.* **81** 1201
- [20] Haskell B A, Wu F, Matsuda S, Craven M D, Fini P T, DenBaars S P, Speck J S and Nakamura S 2003 *Appl. Phys. Lett.* **83** 1554
- [21] Sun G and Khurgin J B 1993 *IEEE J. Quantum Electron.* **29** 1104
- [22] Iizuka N, Kaneko K, Suzuki N, Asano T, Noda S and Wada O 2000 *Appl. Phys. Lett.* **77** 648
- [23] Heber J, Gmachl C, Ng H and Cho A 2002 *Appl. Phys. Lett.* **81** 1237
- [24] Suzuki N and Iizuka N 1998 *Jpn. J. Appl. Phys.* **37** L369
- [25] Jovanović V, Indjin D, Ikončić Z, Milanović V and Radovanović J 2002 *Solid State Commun.* **121** 619
- [26] Capasso F, Paiella R, Martini R, Colombelli R, Gmachl C, Myers T L, Taubman M S, Williams R M, Bethea C G, Unterrainer K, Hwang H Y, Sivco D L, Cho A Y, Sergent A M, Liu H C and Whittaker E A 2002 *IEEE J. Quantum Electron.* **38** 511
- [27] Barbieri S, Alton J, Beere H E, Fowler J, Linfield E H and Ritchie D A 2004 *Appl. Phys. Lett.* **85** 1674
- [28] Kumar S, Williams B S, Kohen S, Hu Q and Reno J L 2004 *Appl. Phys. Lett.* **84** 2494
- [29] Williams B S, Kumar S, Callebaut H, Hu Q and Reno J L 2003 *Appl. Phys. Lett.* **83** 5142
- [30] Hsu L and Walukiewicz W 1997 *Phys. Rev. B* **56** 1520